X-ray Structure of Motor and Neck Domains from Rat Brain Kinesin[†,‡]

Stefan Sack,[§] Jens Müller,[§] Alexander Marx,[§] Manfred Thormählen,[§] Eva-Maria Mandelkow,[§] Scott T. Brady,[||] and Eckhard Mandelkow*[,§]

Max-Planck-Unit for Structural Molecular Biology, c/o DESY, Notkestrasse 85, D-22607 Hamburg, Germany, and Department of Cell Biology, University of Texas Southwestern Medical Center, Dallas, Texas 75235

Received September 10, 1997; Revised Manuscript Received October 16, 1997[⊗]

ABSTRACT: We have determined the X-ray structure of rat kinesin head and neck domains. The folding of the core motor domain resembles that of human kinesin reported recently [Kull, F. J., et al. (1996) *Nature 380*, 550−554]. Novel features of the structure include the N-terminal region, folded as a β-strand, and the C-terminal transition from the motor to the rod domain, folded as two β-strands plus an α-helix. This helix is the beginning of kinesin's neck responsible for dimerization of the motor complex and for force transduction. Although the folding of the motor domain core is similar to that of a domain of myosin (an actin-dependent motor), the position and angle of kinesin's neck are very different from those of myosin's stalk, suggesting that the two motors have different mechanisms of force transduction. The N- and C-terminal ends of the core motor, thought to be responsible for the directionality of the motors [Case, R. B., et al. (1997) *Cell 90*, 959−966], take the form of β-strands attached to the central β-sheet of the structure.

The movement of vesicles or organelles along microtubules is achieved by means of motor proteins such as kinesin or dynein (*1*, *2*). They possess a head domain that attaches to microtubules and hydrolyzes ATP, leading to a conformational switch that converts chemical into mechanical energy. The switch is transmitted via flexible and stiff lever arms ("neck", "stalk") to the cargo (Figure 1). While a single head domain is thought to be competent for force generation, microtubule motor proteins usually have paired motor domains, possibly because this allows them to "walk" along the microtubule surface without losing touch [as in the "hand-over-hand" model of movement (*3*)]. The general principle of transmission of nucleotide-induced conformational changes is realized in a variety of ways, but often with similarities in underlying structures; examples are the actin-based motor proteins (myosin) or signal transduction molecules (G-proteins) (*4*−*6*). Kinesin and kinesin-related microtubule motors provide an intriguing variation on the theme: Similar motor domains can generate opposite movement, toward the anterograde or retrograde end of microtubules. Examples are different kinesin-related proteins such as the *Drosophila* ncd motor (*7*). The basis for this difference lies in the head domain (*8*), specifically in conserved sequences at the N- or C-terminal ends of the motor core domain (*9*, *10*).

An important step toward elucidating the structural basis of microtubule motors was the recent X-ray structure analysis of the human kinesin and the *Drosophila* ncd motor domains (*11*, *12*). The two structures reveal a compact, triangular-shaped head with a central β-sheet sandwiched between α-helices. The protein fragments contain 349 (kinesin) or 366 (ncd) residues, of which about 88% could be traced. The rest was not visible because of intrinsic disorder (N- and C-terminal region, loop L11). The ATP binding site was identified and showed a P-loop arrangement similar to those of other nucleotide binding proteins such as the G-proteins or myosin (*13*−*15*), a feature that had been predicted from the sequence (*16*). The microtubule binding region is presently not well-defined but has been inferred by arguments based on sequence conservation and effects on motility and ATPase [e.g., loops L7−β5−L8a around residue 150, loop L12 around residue 275 (*17*)]. A striking feature is the similarity of both microtubule head domains to part of the actin-based motor myosin (*4*, *18*). The common structure covers a region where conformational switches are likely to occur, but it does not allow an extrapolation to the interface between the motor and its track because myosin has an intervening domain which binds to actin. Such a domain is not present in the microtubule motors. In addition, the myosin structure reveals an α-helical tail stabilized by calmodulin-like "light chains", whereas the α-helical neck or stalk domains of microtubule motors were not included in the initial structures.

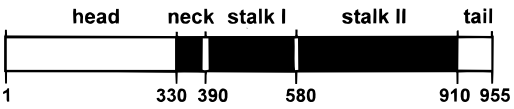

FIGURE 1: Bar diagram of kinesin domains. Rat kinesin contains 955 residues. There are three major domains, the head (1−330), rod (330−910), and tail (910−955). The minimal motor domain (head) is roughly globular, the rod is mostly α-helical coiled coil (shaded domains), and the tail is again globular. The rod can be further subdivided into the neck (340−390) and stalk domains I and II, separated by nonhelical hinges around residues 390 and 580 (a further gap in the coiled-coil prediction lies around residue 820). The prediction was calculated using the program Paircoil (*64*). The kinesin construct used in this study contains the head and the beginning of the neck helix.

[†] This research was funded by grants from the Deutsche Forschungsgemeinschaft (to E.-M.M.), the BMBF (to E.M.), a fellowship of the Friedrich-Ebert-Foundation (to S.S.), and grants from the National Institute of Neurological Disease and Stroke (NS23868 and NS23320) and the Welch Foundation (No. 1237) to S.T.B.

[‡] Atomic coordinates have been deposited in the Protein Data Bank (accession code: 2kin).

* To whom correspondence should be addressed. Phone: (++49)-(40)8998-2810. E-mail: mand@mpasmb.desy.de.

[§] Max-Planck-Unit for Structural Molecular Biology.

[||] University of Texas Southwestern Medical Center.

[⊗] Abstract published in *Advance ACS Abstracts,* December 1, 1997.

S0006-2960(97)02249-6 CCC: $14.00

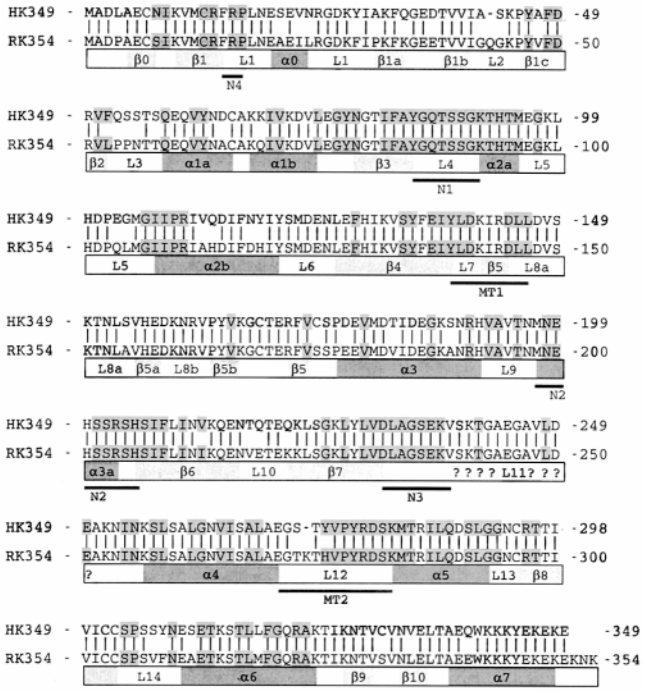

FIGURE 2: Sequence of the rat kinesin head domain (354 residues, line 2) used in this study (Brady, unpublished) compared with the sequence of human kinesin (line 1, ref *21*). Vertical bars indicate sequence identity. Residues highly conserved in the kinesin family are shaded (*12*). The bar shows the secondary structure elements (β = β-strand, α = α-helix, L = loop). The line below the bar indicates motifs involved in nucleotide binding (N1−N4) and microtubule binding (MT1, MT2). As a result of a nucleotide exchange during PCR cloning, in the construct used for this study Gly293 is mutated to Asp. This was detected in the electron density and confirmed by sequencing.

Starting from the cloned rat brain kinesin heavy chain (Brady, unpublished) we have initiated a structure analysis of head domains of different sizes. A 354-residue construct (Figure 2) remains monomeric in solution whereas larger constructs tend to dimerize. Both the monomeric and dimeric head domains have been crystallized (*19*). In this report we describe the structure of the monomeric rat kinesin head refined to 2 Å resolution, whereas the structure of the dimer will be reported elsewhere. Overall, the structure of the rat kinesin monomer is similar to that of the human kinesin. Notable additional features are an N-terminal β-strand, two C-terminal β-strands, and an α-helix which belongs to the neck region and projects away from the bulk of the head. The orientation of the neck is different from the one expected from the "lever arm" helix of myosin, suggesting that the two motors have different mechanisms of transmitting force.

MATERIALS AND METHODS

Cloning, Expression, and Purification of the Rat Brain Kinesin Head Domain. Details of cloning, expression, and crystallization are given elsewhere (*19*). Briefly, a pET expression vector (*20*) coding for the first 354 amino acids of rat kinesin was constructed starting with a full-length rat kinesin cDNA clone (coding for 955 residues; Brady, unpublished). Due to bacterial processing, Met1 is missing on the protein level. Rat brain kinesin is highly homologous to other mammalian kinesins, e.g., human kinesin (*21*) (see Figure 2). The protein was expressed in *Escherichia coli* strain BL21(DE3). Cells, grown in 10 L LB media supplemented with 50 mg/L ampicillin, were induced at A_{600} = 0.6−1.0 with 0.4 mM isopropyl β-D-thiogalactopyranoside (IPTG) for 16 h at room temperature. Packed cells were resuspended in 50 mL of lysis buffer (50 mM Pipes, pH 6.9, 1 mM EGTA, 1 mM DTT, 1 mM $MgCl_2$, 0.5 mM PMSF, 20 μM MgATP), and lysates were prepared using a French press cell. The expressed kinesin fragment was purified by two ion-exchange columns (phosphocellulose and MonoQ) using KCl to eluate the protein. Subsequently, the kinesin motor domain-containing fractions were pooled, concentrated using Ultrafree 30 concentrators (Millipore), and applied to a gel filtration column (G200 Hiload 16/60, Pharmacia) equilibrated with 20 mM Pipes, pH 7.5, 1 mM EGTA, 1 mM DTT, and 100 mM KCl. Peak fractions were pooled, concentrated to about 25 mg/mL, and stored at −70 °C until use.

Table 1: Crystal and Data Collection Parameters

space group	$P2_12_12_1$
unit cell parameters	a = 71.556 Å, b = 73.674 Å, c = 74.128 Å, $\alpha = \beta = \gamma = 90°$
resolution range	40−1.9 Å
total observations	301422
unique reflections	32107
completeness	99.3%
R_{sym}	0.048
$I/\sigma(I) > 2$ fraction	91.1%

Crystallization. Crystallization was done by the hanging drop method. The mother liquor (10 μL) contained 9−14 mg/mL protein, 20 mM Pipes, pH 7.5, 50 mM KCl, 1 mM EGTA, 1 mM DTT, and 0.9 M lithium sulfate. The reservoir was 1.8 M lithium sulfate in the same buffer. Crystals appeared within 2 days at 19 °C.

X-ray Data Collection. Screening for crystal quality was done on a rotating anode X-ray generator (Rigaku RU200) equipped with an image plate detector (MarResearch, Hamburg). Since the crystals were radiation sensitive, they were prefrozen in liquid nitrogen and exposed to X-rays in a stream of cold (−190 °C) nitrogen gas using 30% erythritol (Sigma) as a cryoprotectant. With this system the crystals diffracted to a resolution of up to 2.2 Å. Higher resolution data were obtained on synchrotron beamlines at DESY [Hamburg; wiggler beamlines BW7a and BW7b (EMBL) or BW6 (MPG)]. Under these conditions the best diffracting spots extended to a resolution of 1.7 Å. A complete data set was collected at 1.9 Å resolution. The crystals belong to space group $P2_12_12_1$ with a = 71.56 Å, b = 73.67 Å, c = 74.13 Å, and $\alpha = \beta = \gamma = 90°$. Data reduction was performed using the programs Denzo and Scalepack (*22*). The data collection statistics are summarized in Table 1.

Structure Determination. The structure was solved using molecular replacement methods. Assuming one monomer per asymmetric unit with a molecular mass of 39.7 kDa, the Matthews parameter (*23*) was V_M = 2.46 Å^3/Da, corresponding to a solvent content of 49.6%. An incomplete model of the dimeric form of kinesin (*24*) built from a 3.0 Å MIR map was used as a search model to obtain initial phases. The search model consisted of residues 3−236, 263−274, and 276−335. Some out of register errors could be corrected in the course of model building and refinement cycles. The program AMoRe (*25*) readily found a solution with a correlation factor of 50.5% and an R value of 41.9%. X-PLOR (*26*) was used to perform rigid-body refinement. This yielded an R value of 46.9% and an R_{free} value of 47.7%.

Table 2: Refinement Statistics and Quality of Model

data used in refinement	
resolution range	6−2 Å
no. of reflections	25879
atoms in refinement	
protein	2686
solvent	205
ADP	27
SO_4	15
rms deviation	
bonds	0.017 Å
angles	1.7°
temperature factors (Å^2)	
overall	24.3
main chain	22.3
side chain	26.3
water	31.1
ADP	35.1
SO_4	43.9
crystallographic residuals	
R value	19.4%
R_{free} value	25.4%

The obtained map was interpretable, and side chains and carbonyls were visible after the rigid-body step. In this initial map the incomplete starting model could be extended by a few amino acids in the N- and C-terminal regions as well as in the loops.

Refinement. Prior to refinement 10% of the data were randomly chosen and omitted for the calculation of a free *R* value (*27*). A simulated annealing protocol (T_{max} = 4000 K) (*28*) was used to remove possible model bias. Several cycles of simulated annealing refinement were carried out until the crystallographic residuals reached R = 28.8% and R_{free} = 35.5%. After each refinement cycle inspection and manual rebuilding in $3F_o - 2F_c$ and $F_o - F_c$ maps were performed using the program O (*29*). It was possible to remove out of register errors of the search model and to identify a point mutation (G293D). Water molecules were introduced into the structure using Arp (*30*) and programs of the CCP4 suite (*31*). The positions of the waters found by Arp were checked, keeping only water molecules with clear density in the $3F_o - 2F_c$ map and a signal height larger than 3σ in the $F_o - F_c$ map. Further refinement using X-PLOR yielded R = 22.7% and R_{free} = 31.7%. One ADP molecule and three SO_4 entities were added. Two final refinement steps using the maximum likelihood procedure implemented in the program Refmac (*32*) were carried out, resulting in final values of R = 19.4% and R_{free} = 25.4%. The refined model comprises amino acids 2−239 and 252−351. Twelve residues, 240−251 (=loop L11), were not visible, as well as the last three C-terminal residues (352−354). The quality of the model was checked using the program Procheck (*33*) or with information extracted from the Refmac logfile (see Table 2). A Ramachandran plot of ϕ,ψ angles is given in Figure 3; only one residue (Lys274) lies in a generously allowed region, and none are in disallowed regions.

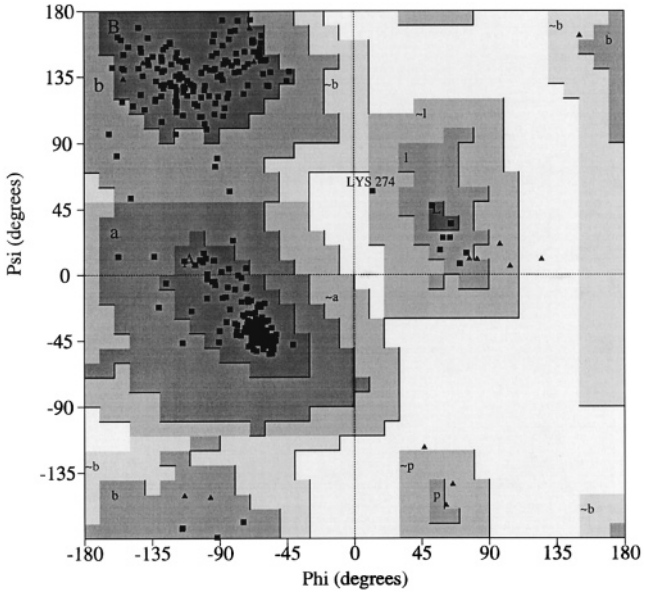

FIGURE 3: Ramachandran plot of the kinesin head domain generated with the program Procheck (*33*). 92.4% (281 residues) are in the most favored regions, and 7.2% (22 residues) are in additional allowed regions. Only Lys274 in the poorly ordered loop L12 lies in a generously allowed region; none are in disallowed regions. Triangles represent glycines.

RESULTS

The domain composition of rat brain kinesin (Figure 1) is similar to that of human kinesin (*21*), with 76% identity overall, rising to 88% in the head domain. As shown by the sequence alignment (Figure 2), rat kinesin contains two inserted residues (Gln43 in loop L2, Lys274 in loop L12) so that the last residue of the human kinesin construct used in ref *11* (residue 349) corresponds to residue 351 of rat kinesin. The first residue of the rat construct is absent due to cleavage during bacterial expression (*34*). As expected from the sequence homology, the parts visible in both the human and rat kinesin structures are similar as well. Figure 4, panels a and b shows the molecule in our reference orientation where one observes the core β-sheet roughly face-on, and the helices α1−α3 are in front of the central β-sheet. In this view the structure has a triangular shape, it resembles a "flower bouquet" bound at the bottom. Figure 4c shows a stereoview of the back side, after rotation by 180° around the vertical axis, so that helices α4−α6 are in the foreground. Figure 5 gives a more detailed overview of the model. The reference view is shown magnified in Figure 5a, with structural elements labeled. The view of Kull et al. (*11*) (their Figure 1) is generated by rotating Figure 5a about 90° around the vertical axis so that the strands on the right are viewed roughly edge-on (Figure 5b). To facilitate the comparison, we will adhere largely to the terminology of β-strands, α-helices, and loops introduced by Kull et al. (see Figure 2).

The structure can be described as an α/β protein (for topology, see Figure 6). There is a core β-sheet of eight β-strands (strands β1−β8) sandwiched between six α-helices (α1, α2, α3 in front of the core sheet, α4, α5, α6 in the back). The sequence of the core strands is (from left to right) β2-β1-β8-β3-β7-β6-β4-β5. Six of them point "up" (β2, β1, β8, β3, β7, β4) and two point "down" (β6, β5). The sheet contains a gradual twist so that the top of the strands on the left leans toward the observer in Figure 4b or Figure 5a, and the ones on the right lean away. This twist is better seen in the top view (Figure 5c). The structure contains three regions of short interrupted β-strands. The minor lobe at the upper left of Figures 4b and 5a is formed by the strands β1a, β1b, and β1c. This is the area where the corresponding stalk of myosin would emanate (see below). Another set of short β-strands is that of β5 (upper and lower part), β5a and

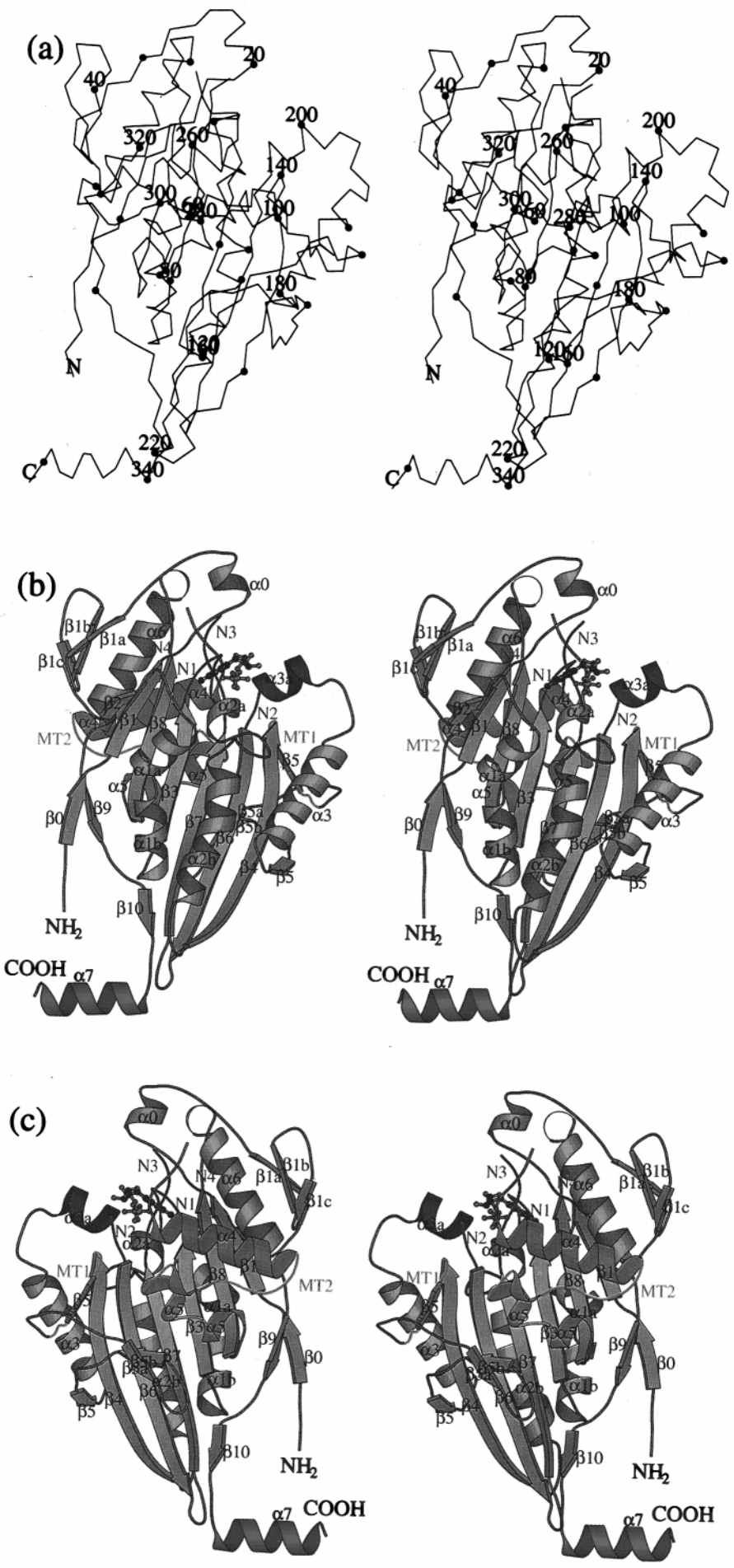
(a)
N
C
(b)
MT1
MT2
NH2
COOH
(c)
MT1
MT2
NH2
COOH

FIGURE 4: Stereoviews of rat kinesin. (a) Backbone C^{α} positions in reference orientation (front view). Every 10th residue is marked with a dot, and every 20th residue is labeled. The structure includes residues 2−239 and 252−351. Residue 1 is missing due to bacterial processing, and residues 240−251 (loop L11) and 352−354 are not visible due to disorder. (b) Ribbon representation in reference orientation. β-Strands are in light blue, and α-helices are in pink (α0−α3, α6), purple (α3a), green (α4, α5), or red (α7). Strands and helices are numbered as in the text (the strand sequence is 2-1-8-3-7-6-4-5, from left to right). This view shows the core β-sheet roughly face-on. It illustrates the topology of the β-strands, particularly the interactions between N-terminal and C-terminal strands (β0 with β9, β1 between β2 and β8, β10 with β7). The bound nucleotide is centered at the top. It is surrounded by loops (purple) containing sequence motifs involved in nucleotide binding and conformational switching (*12*) (see also Figure 5). From left to right, they are at the upper end of strands β1, β3, β7, and β6, containing motifs N4, N1, N3 = switch II and N2 = switch I. The neck helix α7 is in red and projects to the left at the bottom. Regions thought to be involved in microtubule binding are colored green (on the back, loop L7−β5−L8a = MT1, loop L12 and adjacent helices α4 and α5 = MT2; see panel c). The coloring scheme is retained throughout the figures. (c) Ribbon representation of back side, i.e., reference orientation rotated by 180° about the vertical axis. This view shows the presumptive interaction sites with microtubules (green): loops L7−β5−L8a following strand β4 on the left; loop L12 and adjacent helices α4 and α5 in the center. Cartoons were created using Molscript (*65*).

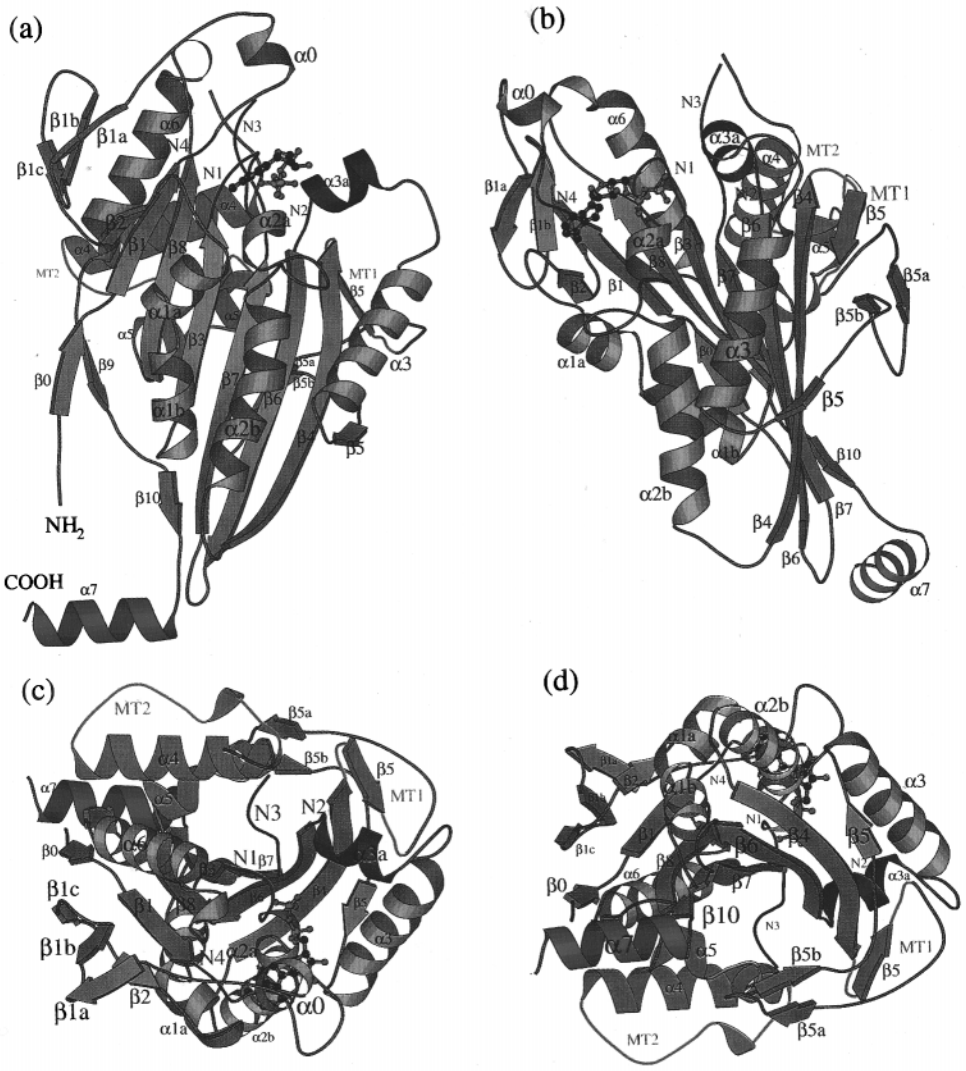

FIGURE 5: Special views of the structure. (a) Reference view (as in Figure 4b), with structural elements labeled. (b) View as in Figure 1 in ref *11*. This view is generated by rotating panel a by about 90° around the vertical axis. Thus the right part of the core sheet is seen roughly edge-on, and the neck helix points away from the observer. (c) View from top, i.e., reference orientation of panel a rotated by 90° around the horizontal axis. Note that the presumptive microtubule interaction sites (green, L7−β5−L8a, L12, and adjacent helices α4 and α5) and the neck helix α7 (red) lie roughly in a common plane on the back side of the core sheet (top in this view). (d) View from bottom, i.e., reference orientation rotated by −90° around the horizontal axis. This view shows the twist of the core sheet: the strands on the right have the opposite inclination from the strands on the left.

β5b on the left of Figure 4c where one of the microtubule interaction sites is thought to occur. A third such region contains β0, β9, and β10, the area of the N- and C-terminal ends of the head.

The nucleotide binding site (ADP in our case) is seen at the top center in Figure 4b. It is surrounded by several loops emanating from strands β1, β3, β7, and β6 (from left to right, colored purple). The chain folding around the nucleotide is comparable to other nucleotide binding proteins, particularly G-proteins (*12*). The analogous regions are termed N4, N1, N3, and N2 (from left to right in Figure 5, panels a and c). They include highly conserved regions such as the beginning of loop L1 (N4) interacting with the adenine base (motif RxRP), the phosphate binding loop (P-loop, loop L4 or N1, motif GxxxxGK), and two "switch" regions (switch II = N3 after β7, motif DLAGSE, and switch I = N2 at the

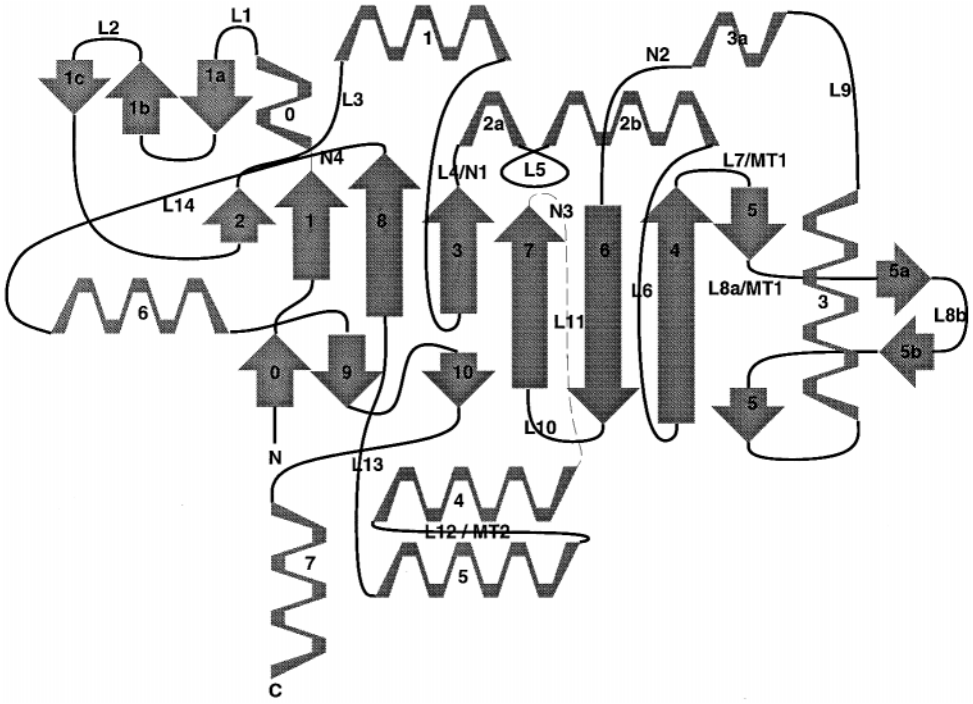

FIGURE 6: Topology of secondary structure elements. The view of the core β-sheet corresponds roughly to the front view of Figure 5a. The nucleotide binding motifs N1−N4 and the presumptive microtubule binding sites MT1 and MT2 are indicated.

transition from α3a to β6, motif SSRSH). A comparison of the eight P-loop residues (GxxxxGKS/T) in kinesin and several other nucleotide binding proteins [e.g., myosin (*35*), transducin (*36*), or $p21^{ras}$ (*13*)] revealed virtually identical positions of the C^{α} atoms (rms values between 0.15 and 0.45 Å).

The nucleotide base is coordinated by His94 forming a stacking interaction with the purine ring and by loop L1 (nucleotide binding region N4). In N4 the second arginine (Arg16) forms a hydrophobic contact with the base, similar to the corresponding Asn127 position in myosin (*35*) or Lys117 in $p21^{ras}$ (*13*). In kinesin the position of Arg16 is additionally stabilized through a salt bridge to Glu22. A hydrogen bond to the O_4 of the ribose is not observed. The conserved Pro17 shows a hydrophobic interaction with the purine ring as described (*11*), superimposing to the Pro128 of chicken skeletal myosin (*15*). The role of the conserved Arg14 may be to shield the base against the solvent. Interestingly, a salt bridge is formed between Glu237 and Arg204, corresponding to Glu459 and Arg238 in the MgADP·AlF_4 structure of myosin connecting N2 and N3 (*35*). This is in contrast to the MgADP·BeF_x structure of myosin and the structure of human kinesin where a connection between Glu199 and Arg203 (corresponding to Glu200 and Arg204 in rat kinesin) is observed. These regions are thought to mediate conformational changes during the nucleotide hydrolysis cycle in G-proteins, myosin, and kinesin (reviewed in refs *4*, *5*, and *37*).

The folding of the core sheet and helices is surprisingly similar to a domain of myosin (*11, 12*). Little experimental evidence is available for the interaction site with microtubules, but arguments based on sequence conservation, charge distribution, and motility place the interaction sites at the back of the molecule of Figure 4b, or the front of Figure 4c, at loops L7−L8a (terminating with the conserved motif DLL), and at L12 [containing the conserved VPYR (*17*)]. Because of the homologies of the two kinesin structures, we will not dwell on the similarities with G-proteins and myosin in more detail; instead, we will concentrate on novel aspects where the two structures differ.

The most prominent differences are at the N- and C-terminal ends of the molecule which contain the residues responsible for the directionality of the motors (*9*). The regions are disordered in the structure of Kull et al. but ordered in our case, i.e., the initial 6 and the final 24 residues. This is presumably due to differences in the packing of the molecules in the crystal lattice (see below, Figure 7). The N- and C-terminal ends are most visible in the reference view (Figure 4b) and are represented schematically in Figure 6. The N-terminal 20 residues adopt an extended conformation traversing the molecule from bottom to top. It contains a short and a longer β-strand ($\beta0$ = Ala5−Cys7, $\beta1$ = Ile9−Phe15) separated by a kink at Ser8. The lower part ($\beta0$) forms an antiparallel β-sheet with strand $\beta9$, linking the N-terminal to the C-terminal region. The upper part ($\beta1$) has parallel strand interactions within the core sheet (between $\beta2$ and $\beta8$).

The second major difference is the C-terminal sequence 328−354. Residues 328−336 form two β-strands ($\beta9$, $\beta10$) interrupted by a kink at Ser332. The upper part ($\beta9$) interacts with strand $\beta0$ in an antiparallel fashion, as mentioned above. The lower part ($\beta10$) is connected to strand $\beta7$ of the core sheet (also antiparallel). Thus the N- and C-terminal ends of the head domain stabilize each other in a dual fashion, directly via the $\beta0-\beta9$ interaction and indirectly via the $\beta10-\beta7$ connection to the core sheet.

From Ala339 on the C-terminal region becomes an α-helix which projects away from the head domain. The direction of the helix is roughly in the plane of the core β-sheet, across the strands (i.e., parallel to the plane of the paper and horizontal in Figure 4, panels b and c). The last three residues (352−354) are too disordered to be traced with certainty. Helix $\alpha7$ is clearly not part of the core but the beginning of a separate domain. The structure agrees well

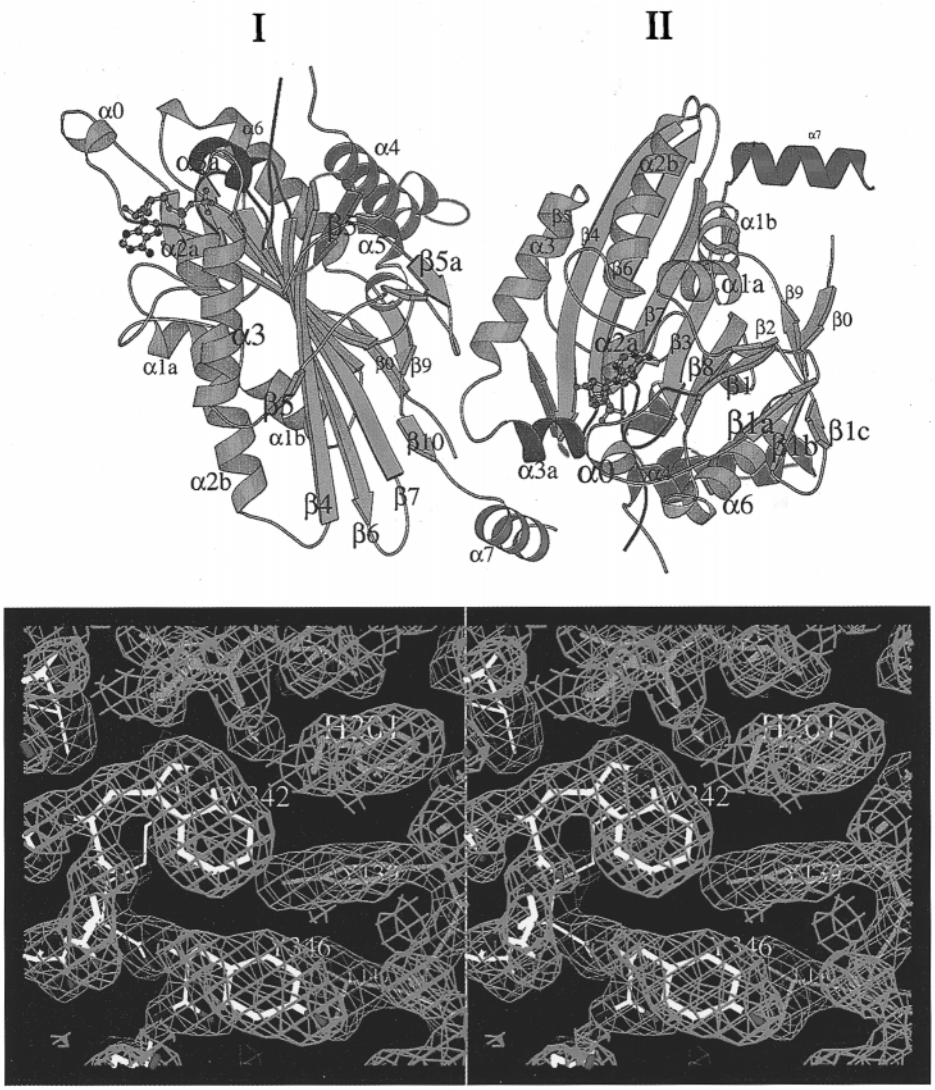

FIGURE 7: Packing of kinesin head domains in the crystal structure. (a, top) Two adjacent kinesin molecules are shown in ribbon representation, illustrating how the N- and C-terminal regions of the left molecule are stabilized in the crystal since they "lean" against the protrusion formed by region α3−L9−α3a and the end of β4−L7−β5. The neck helix α7 of molecule I is juxtaposed to helix loop L7 and α3a of molecule II; the N-terminus of I interacts with loop L9 of II; loop L8b of I approaches helix α3 of II. Additional contacts exist with other neighboring molecules (not shown). Plot created using Molscript (*65*). (b, bottom) Stereo plot of electron density in the contact region between the neck helix α7 of molecule I (left) and the neighboring molecule II. The left shows in yellow Trp342 and Tyr346 (neck helix of molecule I). The right shows in brown His201 (helix α3a of molecule II), Tyr139, and Leu140 (loop L7). The density represents a $2F_o - F_c$ map contoured at 1σ. Figure created using O (*29*).

with biochemical data showing that the motor domain comprises about 340 residues, followed by a rod domain with an α-helical coiled-coil structure (Figure 2). Thus, helix α7 may be regarded as the beginning of the rod domain, specifically the neck.

The close apposition of the N- and C-terminal strands of the head domain is remarkable. It explains why motor domains of different kinesin family members can be placed in different locations of the chain and yet retain their function [at the N-terminus as in kinesin, at the C-terminus like ncd, or elsewhere (*8*, *38*)]. The motor domain is "suspended", as it were, at the β0−β9 junction.

Figure 5, panels c and d, shows the structure in the perspective from the top and bottom, i.e., corresponding to the reference orientation rotated by 90° toward or away from the observer around a horizontal axis. Both views show that the microtubule interaction sites are clustered on one side of the central sheet and that the neck helix β7 lies essentially within the same plane. This has consequences for models of force transduction (as discussed later). These views also show the twisting of the central sheet as one traverses from left to right. The topology of the connections between β-strands and α-helices is summarized in the diagram of Figure 6, which emphasizes the connections of the N- and C-terminal β-strands to the core sheet.

Why are the N- and C-terminal ends of the head domain visible in our structure but disordered and invisible in the model of Kull et al.? The likely answer is the packing of the molecules in the crystal, which is different in the two cases. Figure 7a shows how two adjacent molecules pack against one another with complementary surfaces. The neck helix α7 of the left molecule leans against loop L9−α3a and L7 of the right molecule, the N-terminal residues of the left fit against loop L9 on the right, and loop L8b on the left approaches helix α3 on the right. There are a number of other contacts between these and other adjacent molecules which are not shown here. The tight packing of the two molecules is illustrated in the stereo plot of Figure 7b

showing how Trp342 and Tyr346 of helix α7 fit against His201 (in α3a) and Tyr139 and Leu140 of loop L7 in the neighboring molecule.

DISCUSSION

Kinesin is a motor protein that pulls vesicles or organelles along microtubules, derives its energy from the hydrolysis of ATP, binds preferentially to β-tubulin, and steps along microtubules in 8 nm intervals with pN forces (*1, 2*).

Three-dimensional image reconstructions revealed low-resolution views of the kinesin−microtubule complex, both of monomeric kinesin or ncd (*39*−*41*) and of dimeric forms (*42*−*44*). The crystal structures of kinesin and ncd head domains have been solved at high resolution (*11, 12*). They revealed a surprising similarity with G-proteins and myosin, an actin-based motor protein. These features, their implications for nucleotide-dependent switching, and implications for force transduction by lever arms have recently been reviewed (*4, 5, 37*). As far as we can judge, our kinesin structure is very similar to that of Kull et al. (*11*), and therefore the comparison of the core domain with G-proteins and myosin applies as well. However, the presence of additional structural details in our rat kinesin structure indicates that some elements diverge from both myosins and G-proteins. These differences impose constraints on formulating models for the mechanisms of force transduction. In the following discussion, we concentrate on novel aspects resulting from the parts of our structure that were not visible previously, i.e., the N- and C-terminal regions of the kinesin head.

Relationship between the Motor Domain and Rod Domain of Kinesin. Previous biochemical and electron microscopic studies have subdivided the kinesin domains into "head" (residues 1−340), "rod" (residues 340−910), and "tail" (residues 910−955, the C-terminal end in the case of rat kinesin). The head constitutes the minimal microtubule and ATP binding unit, but it cannot generate movement in vitro without at least some rod-like attachment (*8*). The rod domain is largely α-helical and forms a coiled coil, in agreement with predictions from the sequence and electron microscopy (*45*). It is convenient to subdivide the rod into three parts (Figure 1): the neck, residues 340−390, connecting the motor domain with the first hinge (around 380−390), stalk I (390−580), and stalk II (580−910).

The structure presented here extends to residue 351 (the last three residues are disordered) and therefore covers the head−neck junction. We can therefore ask, how do the earlier conclusions (based on methods such as biochemistry, spectroscopy, or directed mutagenesis) compare with the actual structure? Is the neck really helical? What is its orientation relative to the motor domain?

The polypeptide chain emerges from the core of the head domain in β-strands β9 and β10 and helix α7 (Figures 4b and 5a). Both β9 and β10 are connected to other β-strands of the core head (β9−β0, and β10−β7). If we define the neck as the region where the chain loses its immediate contact with the bulk of the head, this means that the transition zone between head and neck is in the region 336−340, just preceding α7. The neck helix starts at Ala339, and the region 339−354 covers roughly the first half of the stretch Ala339−Trp370, which has a predicted coiled-coil structure because of the heptad repeats (*46*). Strictly speaking, the heptads begin already at Leu335 so that the observed α-helix lags behind the prediction by one turn. The residues between Lys325 (the end of helix α6) and Ala339 (beginning of α7) are in extended or β-conformation, in good agreement with spectroscopic observations on related peptides (*47, 48*). In general, the coiled-coil potential of the region 339−354 is rather weak, presumably because of the unusual density of charged residues and the nonstandard residues in heptad positions. This explains why constructs of similar lengths do not dimerize (*46, 49, 50*). Dissociation constants become low enough for dimerization (below micromolar) only when the constructs reach lengths of 365 or more because the second half of the heptad region (355−370) has a more conventional leucine zipper-like appearance (*47, 48*). In agreement with this, the longer construct rK379 forms a dimer in solution and in the crystals (*19*).

The initial direction of the neck helix is roughly parallel to the plane of the adjacent core sheet of the motor domain, in a direction across the strands (Figure 4b,c). However, the connection to the bulk of the head via β9 and β10 appears quite loose so that it is conceivable that a change in direction might take place at the β10−α7 junction during the ATPase cycle or the power stroke. This could explain the "swivelling" of kinesin motors attached to microtubules (*51*).

Microtubule Binding Site. It is interesting to consider the disposition of the presumptive microtubule binding regions of the kinesin head (MT1 and MT2, green) compared with the force-transducing stalk (α7, red). No canonical microtubule binding sequence or motif has emerged from studies of microtubule binding proteins in general. However, the presence of highly conserved sequences in kinesin family motor domains that are not involved in nucleotide binding or hydrolysis has been used to identify candidate sequences (*12, 17*). By sequence conservation, these potential microtubule interaction sites are in the region of L7−β5−L8a and L12. These motifs form a patch on the upper part of the back side (green in Figure 4c). Remarkably, the C-terminal helix α7 lies in the same rear plane of the molecule, about 3 nm lower (compare top or bottom view of Figure 5c,d). If the upper patch was attached to the microtubule surface, the neck helix would run along the microtubule surface as well. This is at odds with what one would expect for a lever action where the force transducer would need to point away from the microtubule surface. This orientation is the case for myosin and indeed for most models proposed for kinesin movement. The observation implies either that the microtubule binding surface of kinesin is different from that predicted by sequence conservation or alternatively that the C-terminal helix has a different direction in the crystal structure than during actual movement. To point away from the presumed microtubule interacting surface, the helix would have to swing by about 90° so that it would point toward the observer in the reference view (Figures 4b and 5a).

Suspension of the Head on the Kinesin Rod and Motor Directionality. One of the puzzling features of kinesin-like motor domains is that they can be integrated at different points of the chain and yet retain their directionality of movement (*8*). This implies that the directionality is determined at or near the motor domain and does not result from the arrangement of head and rod. The structural basis for this is evident from the model where the entrance (N-terminal) and exit (C-terminal) from the motor domain are closely associated; in fact, β-strands β0 and β9 interact with

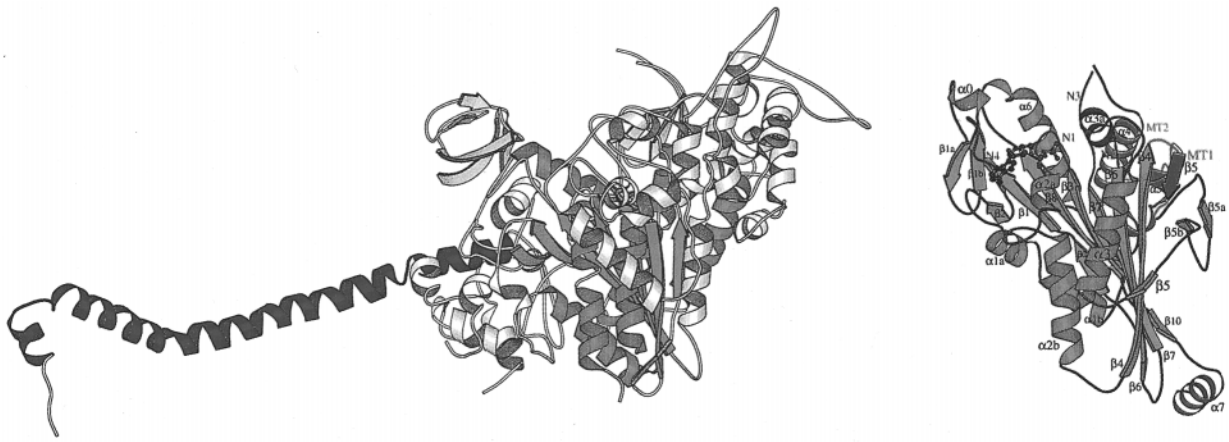

FIGURE 8: Comparison between myosin (PDB entry 2mys, ref *15*) and kinesin and relationship with α-helical tails. The common structure elements are color coded as in Figure 4. The light chains are omitted from the myosin structure. The view is roughly as in ref *18*, the orientation of kinesin is similar to that in ref *11* (see Figure 5b). The α-helical tail of myosin (red) points to the left in the plane of the paper, emanating from the globular domain at the upper left side, roughly where kinesin has its minor lobe around *β*-strands 1a, 1b, and 1c. In the same orientation, the neck helix of kinesin emanates from the lower right and points roughly perpendicular to the plane of the paper, rotated by about 90° from the myosin stalk. The position of the actin filament would be vertical and on the right of the myosin structure, whereas the direction of the microtubule is unknown.

one another. Moreover, helix α7 extends away from the head. Thus the arrangement appears like a motor budding off from its support line (the rod). The loose nature of head−neck interaction explains why the motor must be capable of determining directions by itself, independently of where it is suspended.

A recent analysis (*9*) has shown that the determinants for the directionality lie in conserved residues close to the entrance and exit to the motor core, behind helix α6 for kinesin (^{325}KxIxxxxxVN^{334} in the rat kinesin sequence) or before the equivalent of *β*1 for ncd. This corresponds to *β*-strand *β*9 for kinesin or *β*0 for ncd (which would be preceded by the equivalent of the neck helix). It is tempting to speculate that the conserved strands mediate an interaction between their adjacent neck helices and the body of the motor domain which determines the directionality.

Relationship of the Crystal Structure with Image Reconstructions. Several groups have recently presented 3D image reconstructions of microtubule walls decorated with either monomeric kinesin or ncd heads (*39*−*41*) or with dimeric heads (*42*−*44*). Some reconstructions revealed projections or spikes extending from the main body of the kinesin head and away from the microtubule surface and were considered as the initial part of the neck moving in a lever-like fashion, reminiscent of the lever of myosin (e.g., Figure 4 in ref *40*). This interpretation is not easily reconciled with the orientation of the neck relative to the presumptive microtubule binding surface observed in the X-ray structure. The binding loops of kinesin cover the back surface of the molecule, and the neck helix α7 lies roughly in the same plane (Figure 5c,d). Given this arrangement one could imagine the neck to project tangentially away from the microtubule surface, but not radially away from it.

A more detailed picture emerged from the comparison of microtubules decorated with ncd and the X-ray structure of ncd (*44*). The image reconstruction showed the rear surface (green in Figure 3) apposed against the microtubule surface, loop L11 wrapping around the protofilament and loops L6 and L10 pointing away from the microtubule surface. If we rotate our observed structure into an equivalent orientation, we find that the neck helix is also tangential to the microtubule surface (since it runs parallel to the rear surface). If one views a microtubule from outside, with plus end down, the orientation of the bound kinesin would correspond roughly to the reference view of Figure 4a. Conversely, if we view the microtubule in standard orientation (plus end up), the view of kinesin would be that of Figure 4a rotated by 180° in the plane of the paper. Thus the neck helix would appear at the upper end of the molecule, pointing to the right (counterclockwise along the microtubule surface). The latter orientation would be consistent with the image reconstructions of microtubules decorated with kinesin or ncd dimers which show the neck (=junction between the two heads) pointing to the right at the upper end of the bound head, seen in front view (*42*, *43*).

Models of the Lever. Perhaps the most intriguing aspect of the kinesin structure is its similarity with part of the myosin structure. In the case of myosin there is considerable evidence suggesting how the nucleotide-dependent conformational changes might be transmitted into the swinging of the α-helical tail, the "lever arm". Crystal structures of myosin with different nucleotide analogs representing different states are available (reviewed in refs *5* and *37*). They suggest how the opening and closing of the nucleotide binding pocket could lead to a rotation of an α-helix which in turn controls the lever. Moreover, the velocity of myosin is directly proportional to the length of the lever arm (*52*, *53*). Since the structure of the kinesin head can be superimposed with the nucleotide binding domain of myosin, it is tempting to speculate that the α-helical lever arm would be in a corresponding position. This analogy has been described in more detail in recent reviews (*4*, *18*).

When one superimposes the kinesin structure with myosin (*15*) (Figure 8), the surprising result is that the neck helix of kinesin is in the opposite position of what one would expect from the analogy with myosin. Moreover, it runs in a different direction relative to the core of the domain, roughly at right angles. In the representation of Figure 8, the myosin rod would project roughly from the minor lobe (upper left) in a horizontal direction, i.e., in the plane of the paper. By contrast, the C-terminal helix of kinesin is on the lower right and points roughly into the plane of the paper. The clear

difference between the structures suggests that the mechanism of force transduction is different as well.

In the case of kinesin there are at least three missing links: (1) Myosin has an extra domain connecting the nucleotide binding domain to the actin filament; this domain is largely absent from kinesin, and thus we do not know whether the kinesin−microtubule orientation is comparable to the myosin−actin orientation. (2) The structure of actin is known (*54*) and has been fitted into the structure of the actin filament (*55*), allowing one to model the myosin−actin interaction. By contrast, the structure of tubulin or microtubules is only beginning to emerge (*56*) so that the kinesin−tubulin interaction will remain a matter of speculation for some time. (3) The kinetics of the myosin and kinesin power cycles are very different: myosin spends most of the cycle detached from the actin filament, is not processive, and does not need to be since there are many other myosins in the neighborhood which sustain movement (for a discussion see refs *57*−*59*). Kinesin, on the other hand, works processively and may require dimers for this (*60*). Thus the current thinking is dominated by "hand-over-hand" or similar models (*3*). When translating this into the structure, one is confronted with the difficulty that kinesin is really too small to walk in 8 nm steps along microtubules with ease, and solutions such as unwinding and rewinding the coiled coil for every step seem hard to prove at this point.

The evidence that kinesin does not have a lever homologous to that seen in myosin makes the situation even more complex. If the neck remains close to the microtubule surface, as suggested by its position relative to the other microtubule binding elements, we may have to consider different kinds of models which do not require extensive levers. One simplification would be to discard the assumption that two heads are an absolute necessity—after all, single-headed kinesin-related proteins have been described and shown to work (*61*). The second would be to assume substeps smaller than 8 nm (following the observations in refs *62* and *63*). The third would be to allow a type of crawling or worm-like motion on the surface without a swinging lever. Such models will obviously depend on further insights in the structure of kinesin dimers and how they interact with microtubules. Regardless, the configuration of the neck region seen in this structure indicates that modeling mechanisms of force transduction by analogy with myosin is not sufficient to understand kinesin-based motility.

ACKNOWLEDGMENT

We thank H.-D. Bartunik, G. Bourenkov, and A. Popov for help with the MPG/GBF beamline BW6, as well as V. Lamzin and the staff of EMBL outstation Hamburg for help with the EMBL beamlines BW7a and BW7b. This work contains parts of the doctoral theses of S.S. and J.M.

REFERENCES

1. Brady, S. T. (1995) *Trends Cell Biol. 5*, 159−164.
2. Hirokawa, N. (1996) *Trends Cell Biol. 6*, 135−141.
3. Cross, R. A. (1994) *J. Muscle Res. Cell Motil. 16*, 91−94.
4. Vale, R. D. (1996) *J. Cell Biol. 135*, 291−302.
5. Rayment, I., Smith, C., and Yount, R. (1996) *Annu. Rev. Physiol. 58*, 671−702.
6. Vale, R. D., and Fletterick, R. J. (1997) *Annu. Rev. Cell Dev. Biol. 13*, 745−777.
7. Moore, J. D., and Endow, S. A. (1996) *BioEssays 18*, 207−219.
8. Stewart, R. J., Thaler, J. P., and Goldstein, L. (1993) *Proc. Natl. Acad. Sci. U.S.A. 90*, 5209−5213.
9. Case, R. B., Pierce, D. W., Hom-Booher, N., Hart, C. L., and Vale, R. D. (1997) *Cell 90*, 959−966.
10. Henningsen, U., and Schliwa, M. (1997) *Nature 389*, 93−96.
11. Kull, F. J., Sablin, E., Lau, P., Fletterick, R., and Vale, R. (1996) *Nature 380*, 550−554.
12. Sablin, E. P., Kull, F. J., Cooke, R., Vale, R. D., and Fletterick, R. J. (1996) *Nature 380*, 555−559.
13. Pai, E., Kabsch, W., Krengel, U., Holmes, K., John, J., and Wittinghofer, A. (1989) *Nature 341*, 209−214.
14. Lambright, D., Sondek, J., Bohm, A., Skiba, N., Hamm, H. E., and Sigler, P. (1996) *Nature 379*, 311−319.
15. Rayment, I., Rypniewski, W. R., Schmidt-Bäse, K., Smith, R., Tomchick, D. R., Benning, M. M., Winkelmann, D. A., Wesenberg, G., and Holden, H. M. (1993) *Science 261*, 50−57.
16. Yang, J., Laymon, R., and Goldstein, L. S. B. (1989) *Cell 56*, 879−889.
17. Woehlke, G., Ruby, A. K., Hart, C. L., Ly, B., Hom-Booher, N., and Vale, R. D. (1997) *Cell 90*, 207−216.
18. Rayment, I. (1996) *Structure 4*, 501−504.
19. Kozielski, F., Schönbrunn, E., Sack, S., Müller, J., Brady, S., and Mandelkow, E. (1997) *J. Struct. Biol. 119*, 28−34.
20. Studier, W. F., Rosenberg, A. H., Dunn, J. J., and Dubendorff, J. W. (1990) *Methods Enzymol. 185*, 60−89.
21. Navone, F., Niclas, J., Hom-Booher, N., Sparks, L., Bernstein, H. D., McCaffrey, G., and Vale, R. D. (1992) *J. Cell Biol. 117*, 1263−1275.
22. Otwinowski, Z., and Minor, W. (1997) *Methods Enzymol. 276*, 307−326.
23. Matthews, B. W. (1968) *J. Mol. Biol. 33*, 491−497.
24. Kozielski, F. (1997) Ph.D. Thesis, Hamburg University.
25. Navaza, J. (1994) *Acta Crystallogr. A50*, 157−163.
26. Brünger, A. T. (1992) *X-PLOR Version 3.1*, Yale University Press, New Haven, CT.
27. Brünger, A. T. (1992) *Nature 355*, 472−474.
28. Brünger, A. T., Krukowski, A., and Erickson, J. (1990) *Acta Crystallogr. A46*, 584−593.
29. Jones, T. A., Zou, J. Y., Cowan, S. W., and Kjeldgaard, M. (1991) *Acta Crystallogr. A47*, 110−119.
30. Lamzin, V., and Wilson, K. (1993) *Acta Crystallogr. D49*, 129−147.
31. Collaborative Computing Project No. 4 (1994) *Acta Crystallogr. D50*, 760−763.
32. Murshudov, G. N., Vagin, A. A., and Dodson, E. (1997) *Acta Crystallogr. D53*, 240−255.
33. Laskowski, R. A., McArthur, M. W., Moss, D. S., and Thornton, J. M. (1993) *J. Appl. Crystallogr. 26*, 283−291.
34. Hirel, P. H., Schmitter, M. J., Dessen, P., Fayat, G., and Blanquet, S. (1989) *Proc. Natl. Acad. Sci. U.S.A. 86*, 8247−8251.
35. Fisher, A., Smith, C. A., Thoden, J. B., Smith, R., Sutoh, K., Holden, H. M., and Rayment, I. (1995) *Biochemistry 34*, 8960−8972.
36. Noel, J. P., Hamm, H. E., and Sigler, P. B. (1993) *Nature 366*, 654−663.
37. Holmes, K. (1997) *Curr. Biol. 7*, R112−R118.
38. Cole, D. G., and Scholey, J. M. (1995) *Trends Cell Biol. 5*, 259−262.
39. Hoenger, A., Sablin, E., Vale, R., Fletterick, R., and Milligan, R. A. (1995) *Nature 376*, 271−274.
40. Hirose, K., Lockhart, A., Cross, R. A., and Amos, L. A. (1995) *Nature 376*, 277−279.
41. Kikkawa, M., Ishikawa, T., Wakabayashi, T., and Hirokawa, N. (1995) *Nature 376*, 274−277.
42. Arnal, I., Metoz, F., Debonis, S., and Wade, R. H. (1996) *Curr. Biol. 6*, 1265−1270.
43. Hirose, K., Lockhart, A., Cross, R. A., and Amos, L. A. (1996) *Proc. Natl. Acad. Sci. U.S.A. 93*, 9539−9544.
44. Sosa, H., Dias, D. P., Hoenger, A., Whittaker, M., Wilson-Kubalek, E., Sablin, E., Fletterick, R. J., Vale, R. D., and Milligan, R. A. (1997) *Cell 90*, 217−224.

45. De Cuevas, M., Tao, T., and Goldstein, L. S. B. (1992) *J. Cell Biol. 116*, 957−966.
46. Huang, T. G., Suhan, J., and Hackney, D. D. (1994) *J. Biol. Chem. 269*, 16502−16507.
47. Tripet, B., Vale, R. D., and Hodges, R. S. (1997) *J. Biol. Chem. 272*, 8946−8956.
48. Morii, H., Takenawa, T., Arisaka, F., and Shimizu, T. (1997) *Biochemistry 36*, 1933−1942.
49. Correia, J. J., Gilbert, S. P., Moyer, M. L., and Johnson, K. A. (1995) *Biochemistry 34*, 4898−4907.
50. Jiang, W., Stock, M. F., Li, X., and Hackney, D. D. (1997) *J. Biol. Chem. 272*, 7626−7632.
51. Hunt, A. J., and Howard, J. (1993) *Proc. Natl. Acad. Sci. U.S.A. 90*, 11653−11657.
52. Uyeda, T. Q., Abramson, P. D., and Spudich, J. A. (1996) *Proc. Natl. Acad. Sci. U.S.A. 93*, 4459−4464.
53. Anson, M., Geeves, M. A., Kurzawa, S. E., and Manstein, D. J. (1997) *EMBO J. 15*, 6069−6074.
54. Kabsch, W., Mannherz, H. G., Suck, D., Pai, E. F., and Holmes, K. C. (1990) *Nature 347*, 37−44.
55. Lorenz, M., Popp, D., and Holmes, K. C. (1993) *J. Mol. Biol. 234*, 826−836.
56. Nogales, E., Wolf, S., Khan, I., Luduena, R., and Downing, K. (1995) *Nature 375*, 424−427.
57. Hackney, D. D. (1996) *Annu. Rev. Physiol. 58*, 731−750.
58. Howard, J. (1996) *Annu. Rev. Physiol. 58*, 703−729.
59. Johnson, K. A., and Gilbert, S. P. (1995) *Biophys. J. 68*, 173−179.
60. Berliner, E., Young, E. C., Anderson, K., Mahtani, H. K., and Gelles, J. (1995) *Nature 373*, 718−721.
61. Nangaku, M., Sato-Yoshitake, R., Okada, Y., Noda, Y., Takemura, R., Yamazaki, H., and Hirokawa, N. (1994) *Cell 79*, 1209−1220.
62. Coppin, C. M., Finer, J. T., Spudich, J. A., and Vale, R. D. (1996) *Proc. Natl. Acad. Sci. U.S.A. 93*, 1913−1917.
63. Gelles, J., Schnapp, B. J., and Sheetz, M. P. (1988) *Nature 331*, 450−453.
64. Berger, B., Wilson, D. B., Wolf, E., Tonchev, T., Milla, M., and Kim, P. S. (1995) *Proc. Natl. Acad. Sci. U.S.A. 92*, 8259−8263.
65. Kraulis, P. J. (1991) *J. Appl. Crystallogr. 24*, 946−950.

BI9722498